

**Covalent conjugates based on nanodiamonds with doxorubicin and a cytostatic drug from  
the group of 1,3,5-triazines: synthesis, biocompatibility and biological activity**

*Vladimir V. Sharoyko<sup>a,b,c1</sup>, Grigory M. Berdichevsky<sup>a</sup>, Lubov V. Vasina<sup>a</sup>, Olga S. Shemchuk<sup>a,b</sup>,  
Dmitriy N. Maystrenko<sup>c</sup>, Oleg E. Molchanov<sup>c</sup>, Abdelsattar O. E. Abdelhalim<sup>b,d</sup>, Alexey V.  
Nashchekin<sup>e</sup>, Dmitry A. Nerukh<sup>g</sup>, Grigori V. Tochilnikov<sup>f</sup>, Igor V. Murin<sup>b</sup>, Konstantin N.  
Semenov<sup>a,b,c1</sup>*

<sup>a</sup>Pavlov First Saint Petersburg State Medical University, L'va Tolstogo str. 6-8, Saint Petersburg, 197022, Russia

<sup>b</sup>Institute of Chemistry, Saint Petersburg State University, Universitetskii pr. 26, Saint Petersburg, 198504, Russia

<sup>c</sup>A. M. Granov Russian Research Centre for Radiology and Surgical Technologies, 70 Leningradskaya Ulitsa, Saint Petersburg, 197758, Russia

<sup>d</sup>Environmental Research Department, National Center for Social and Criminological Research (NCSCR), 4 Agouza, Giza, 11561, Egypt

<sup>e</sup>Ioffe Physical-Technical Institute of the Russian Academy of Sciences, 26 Polytekhnicheskaya 194021 Saint Petersburg

<sup>f</sup>Petrov Research Institute of Oncology, 68 Leningradskaya Street, Pesochny, Saint Petersburg 197758, Russia

<sup>g</sup>Department of Mathematics, Aston University, Birmingham, B4 7ET, The United Kingdom

Word count: 6183

Number of figures: 5

<sup>1</sup>Corresponding authors at: 6–8 L'va Tolstogo ulitsa, Saint Petersburg, 197022, Russia (K. N. Semenov and V. V. Sharoyko)

E-mail addresses: knsemenov@gmail.com (K. N. Semenov), sharoyko@gmail.com (V. V. Sharoyko).

## Abstract

We report the synthesis of covalent conjugates of nanodiamonds with doxorubicin and a cytostatic drug from the class of 1,3,5-triazines. The obtained conjugates were identified using a number of physicochemical methods (IR-spectroscopy, NMR-spectroscopy, XRD, XPS, TEM). The nanodiamonds were investigated biomedically for their hemocompatibility, antiradical activity, mechanisms of endocytosis, and cytotoxicity.

## Key words

Nanodiamond, 1,3,5-triazine, biocompatibility, doxorubicin, cytotoxicity, hemocompatibility, antiradical activity, endocytosis

### *List of abbreviations:*

ND, nanodiamond; Dox, Doxorubicin; substance 1, [5 - [[4,6-bis (aziridine-1-yl) -1,3,5-triazine-2-yl]-amino]-2,2-dimethyl-1,3-dioxane-5-yl]-methanol; EDC, 1-ethyl-3-(3-dimethylaminopropyl)carbodiimide; NHS, N-hydroxysuccinimide; ADP, adenosine diphosphate; DCM, dichloromethane; DMAP, 4-dimethylaminopyridine; aPTT, activated partial thromboplastin time, PT, prothrombin time, TT, thrombin time; HEK293, human embryonic kidney cell line; PANC-1, pancreatic adenocarcinoma; T98G, glioblastoma; HeLa, cervical adenocarcinoma; TEM, transmission electron microscopy; HSA, human serum albumin; MTT, 3-(4,5-dimethylthiazol-2-yl)-2,5-diphenyltetrazolium bromide; PBS, phosphate buffer saline; PRP, platelet-rich plasma; UV, ultraviolet.

## 1. Introduction

Targeted drug delivery is one of the most intensively developed areas of medicine [1–8]. Systems for such delivery help reducing the toxic effects of the drugs by lowering their dosage and increasing their effectiveness by targeting the transport to the location of the pathological process [9–14].

Nanocarriers are good candidates for delivery systems due to their biocompatibility (the lack of immune response upon contact with cells and tissues of a living organism) and ability to biodegrade [15]. Nanodiamonds (ND) [16–22] are currently considered as promising system characterized by high delivery efficiency and low toxicity [23]. Low cost, chemical inertness, and the ability to overcome drug resistance make ND attractive as carriers in antitumor drug delivery systems [6,24–26].

One of the most studied and effective chemotherapy drugs is the anthracycline antibiotic Doxorubicin (Dox) [27]. Unfortunately, the pronounced antitumor effect of Dox is accompanied by significant side effects (nausea, vomiting, alopecia). Along with the general toxic effects patients develop congestive cardiomyopathy and chemoresistance due to the pronounced cardiotoxicity of Dox [27].

The drug also develops resistance to therapy which necessitates the search for new chemicals with cytostatic properties [26–32]. Thus, in 1996, the substance with antitumor activity that belongs to the group of alkylating agents of the ethyleneimine class with antitumor activity that belongs to the group of alkylating agents of the ethyleneimine class was synthesized. Its systematic name is [5 - [[4,6-bis (aziridin-1-yl) -

1,3,5-triazin-2-yl]-amino]-2,2-dimethyl-1,3-dioxan-5-yl]-methanol (Fig. 1) and we will further refer to it as 'substance 1'.

In our group, the investigation of the physicochemical properties (density, viscosity, refraction index, solubility, partition coefficient, etc) as well as the stability of substance 1 solutions at various pH were carried out [33]. Special attention was paid to the study of its biocompatibility and bioactivity. In particular, two main mechanisms of its action were proposed, namely, the intercalation with the DNA molecule and the change of the antioxidant-prooxidant balance in tumor cells [34].

During fragmentary clinical trials conducted in patients with advanced forms of malignant neoplasms of various localizations substance 1 demonstrated its antitumor efficacy. It was shown that the most significant effect was observed in chemotherapy of common forms of epithelial malignant tumors of the ovary at stages III-IV, including those accompanied by ascites, using single doses of 15 mg intravenously by stream or intraperitoneally at intervals of 72-96 h up to a total dose of 90-120 mg. Substance 1 is less toxic than drugs based on platinum coordination complexes (the standard in the treatment of ovarian cancer) and, unlike them, does not cause complications in the form of adhesions. However, a significant side effect of substance 1 is myelosuppression [35].

An alternative strategy aimed at reducing the side effects of antitumor agents is their inclusion in colloidal, nanoscale delivery systems <sup>28-30</sup>. The use of such systems allows in some cases to correct such significant shortcomings of the drug as low stability, rapid metabolism, limited penetration into cells and low intracellular concentrations, and the absence of cell and tissue specificity. We, therefore, set to investigate Dox and substance 1 as their conjugates with ND by studying their synthesis, identification,

biocompatibility.

and

cytotoxicity

## 2. Experimental part

### 2.1 Synthesis

The substances that were used in this work are presented in Table 1.

#### 2.1.1 Amidation reaction of ND-COOH with DOX

Carboxylated ND were provided by Ioffe Physical-Technical Institute of the Russian Academy of Sciences (Saint Petersburg, Russia). 500 mg of ND-COOH were dispersed in deionized water with subsequent addition of 250 mg of EDC and 300 mg of NHS with stirring at room temperature for 2 h at pH 5-6, the pH was adjusted using few drops of HCl. Then 50 mg of Dox dissolved in deionized water were added to the mixture while increasing the pH to 8-9 using NaHCO<sub>3</sub>. The mixture was stirred in darkness for 48 h at room temperature. The powder was isolated by filtration, washed with deionized water and dried at 50 °C (Fig. 2).

#### 2.1.2 Esterification reaction of ND-COOH with substance 1

500 mg of ND-COOH dispersed in DCM and DMAP were dissolved in DCM and stirred with ND-COOH solution for 1.5 h. Then, 50 mg of substance 1 in DCM were added and the mixture was stirred at room temperature in darkness for 48 h. The precipitate was filtered, washed with DCM, and dried at 50 °C (Fig. 3).

#### 2.1.3 Degree of ND loading with cytostatics

The degree of loading was calculated by weighting the samples before and after functionalization:

$$\%loading = \frac{m_{final(ND-cytostatic)} - m_{initial(ND)}}{m_{final(ND-cytostatic)}} \cdot 100\% \quad (1),$$

where  $m_{final(ND-cytostatic)}$  is the mass of the resulting conjugate,  $m_{initial(ND)}$  is the mass of initial ND.

Formatted: Russian

For ND-Dox the degree of loading was 70.0 %, and for ND-substance 1 it was 62.5 %.

## 2.2 Identification

~~A group of~~We used the following physicochemical methods ~~were used~~ to characterize ~~the~~ ~~the obtained~~ ND-Dox and ND-substance 1 ~~conjugates~~: IR spectroscopy (FTIR-8400S spectrometer, Shimadzu, Tokyo, Japan), elemental analysis (Euro EA3028-HT, EuroVector, Pavia, Italy),  $^{13}\text{C}$  NMR spectroscopy (NMR-spectrometer Avance III 400 WB, Bruker, Billerica, Massachusetts, USA), ~~and~~ XPS (Thermo Fisher Scientific ESCALab 250Xi, USA). The morphology of ~~the~~ nanoparticles was determined using ~~a~~-scanning electron ~~microscope~~ ~~microscopy~~ (JSM-7001F scanning electron microscope, Japan).

The size distribution of ND-Dox and ND-Substance 1 particles in the aqueous ~~dispersions~~dispersions and the  $\zeta$ -potentials were ~~studied-measured~~ using Malvern Zetasizer 3000 ~~apparatus~~(Malvern Instruments, Malvern, Worcestershire, United Kingdom).

## 2.3 Biocompatibility study

### 2.3.1 Hemolysis

After obtaining informed consent, blood samples for the study were taken from eight donors of both sexes, ~~aged~~20-30 years ~~old~~. The study of erythrocyte hemolysis was carried out by measuring the optical density of supernatants at  $\lambda = 540 \text{ nm}$  ~~using~~ ~~a~~ Thermo Scientific Evolution 300 spectrophotometer (USA). The reaction mixture was prepared from 1 ml of ND-Dox and ND-substance 1 dispersions at ~~a-the~~ concentration of  $2.5\text{--}25 \text{ mg}\cdot\text{l}^{-1}$  and 1 ml of ~~an~~erythrocyte suspension in ~~an~~-NaCl isotonic solution. After preparation, the samples were incubated at  $37 \pm 0.2^\circ\text{C}$  for 1 and 3 h. After incubation, the tubes were centrifuged for 10 min at 2000 rpm.

### 2.3.2 Platelet aggregation

After obtaining informed consent, blood samples for the study were taken from eight donors of both sexes, ~~aged~~20-30 years ~~old~~, who did not receive drugs that affect platelet function for 7-10 days. To prevent platelet activation, blood was taken into vacuum tubes containing 3.8% sodium citrate ~~in~~-with the sodium citrate: blood ratio ~~of~~1:9. To obtain platelet-rich plasma (PRP), stabilized blood was centrifuged at 3000 rpm for 5 min.



Platelet aggregation in PRP was studied using the platelet aggregation analyzer Solar AP2110 (Republic of Belarus) at the temperature of 37°C; the rotation speed of the magnetic stirrer was 1200 rpm. ADP (final concentration  $C = 10 \mu\text{M}$ ), collagen (final concentration  $C = 2 \text{ mg}\cdot\text{ml}^{-1}$ ) and adrenaline (final concentration  $C = 10 \mu\text{g}\cdot\text{ml}^{-1}$ ) were used as inducers. The effect of ND-Dox and ND-substance 1 on induced platelet aggregation was determined by mixing 270  $\mu\text{l}$  of PRP and 30  $\mu\text{l}$  of ND-Dox and ND-substance 1 dispersions in cuvettes at the final concentrations  $C = 2.5\text{--}25 \text{ g l}^{-1}$ . The inducers were added to the cuvettes 5 min after the mixture was incubated. The kinetics of aggregation was recorded until reaching a plateau on the aggregation curve.

### 2.3.3 Clotting tests

Clotting tests included d methods for measuring aPTT, PT, and TT. These methods allow measuring the time interval from the moment of adding a reagent (an activator that starts the coagulation process) to the formation of a fibrin clot in the plasma under study. To determine aPTT, PT, and TT, the reagent kits from Tekhnologiya-Standard (Russia) were used. The studies were carried out on APG2-02-P coagulometer (EKMO, Russia). For the study, 50  $\mu\text{l}$  of plasma and 50  $\mu\text{l}$  of ND-Dox and ND-substance 1 dispersions were mixed to obtain dispersions with various concentrations in the range  $0.375\text{--}1.5 \text{ g}\cdot\text{l}^{-1}$ .

### 2.3.4 Binding with HSA

The study of the binding of ND-Dox and ND-substance 1 with HSA was carried out using SOLAR CM 2203 spectrofluorimeter (Republic of Belarus). Emission spectra were measured in the wavelength range 310-450 nm at the excitation wavelength of 290 nm; the temperature was  $T = 298.15 \text{ K}$ . To measure the fluorescence spectra, the dispersions containing 3  $\mu\text{M}$  of HSA and 0, 0.005, 0.01, 0.015, 0.02, 0.025, 0.03, 0.035, 0.04  $\text{g}\cdot\text{l}^{-1}$  of ND-Dox and ND-substance 1 were prepared.

### 2.3.5 Cytotoxicity

Formatted: Not Superscript/ Subscript

Cytotoxicity was studied using the MTT test (3-(4,5-dimethylthiazol-2-yl)-2,5-diphenyltetrazolium bromide). The following cell lines were used to evaluate cytotoxicity: PANC-1 pancreatic adenocarcinoma, T98G glioblastoma, and HeLa cervical adenocarcinoma.

The cells were cultured in a CO<sub>2</sub> incubator at 37°C in humidified atmosphere containing air and 5% CO<sub>2</sub> in the DMEM-F12 nutrient medium containing 10% thermally inactivated fetal bovine serum, 1% L-glutamine, 50 U·ml<sup>-1</sup> penicillin, and 50 µg·ml<sup>-1</sup> streptomycin.

For the experiment, the cells were seeded in a 96-well plate and placed overnight in a CO<sub>2</sub> incubator. During this time, the cells attached to the surface of the wells (5000 cells were added to each well in 200 µl of DMEM-F12 medium). The number of cells was counted by the BioRad TC10 cell viability analyzer (Bio-Rad Laboratories, USA), after which the aqueous dispersion of ND and their conjugates with cytostatics was added to the wells in the concentration range of 0.47–30 µg · l<sup>-1</sup>. The cells were incubated in the plates for 48 h in a CO<sub>2</sub> incubator at 37°C. At the end of the incubation period, the DMEM-F12 culture medium was discarded by inverting the plate. Next, 100 µl of DMEM-F12 medium and 20 µl of the MTT reagent were added to the wells, and the plates with the cells were incubated for 1 h in a CO<sub>2</sub> incubator at 37°C. After removal of the supernatant, the obtained formazan crystals were dissolved for 15 min with stirring in 200 µl of DMSO per well, and then the optical density was measured using the BioRadxMarx plate spectrophotometer (Bio-Rad Laboratories, USA) at the wavelengths of 540 nm and 690 nm. To correct for background, the absorbances at 540 nm were subtracted from the absorbances at 690 nm for the respective wells. Data were normalized as percentage relative to the control cells incubated without the addition of the test substances.

### **2.3.6 Endocytosis**

The mechanisms of endocytosis were studied using the MTT test to evaluate the toxic effect of the conjugates on HeLa cells in the presence of the following endocytosis inhibitors: CK-636 (*C* = 150 µM), Nystatin (*C* = 30 µM), Dynasore (*C* = 300 µM), Nydrate (*C* = 10 µM),

Chloropromazine ( $C = 70 \mu\text{M}$ ), and Amiloride ( $C = 150 \mu\text{M}$ ). Cytotoxicity data in the presence of the inhibitors were compared with controls in the absence of the inhibitors.

### 2.3.7 Antiradical activity

Solution of DPPH in ethanol and dispersions of ND-Dox and ND-substance 1 in water were prepared. Then, the solution and the dispersions were mixed in the 1:1 ratio. The concentration of DPPH in the final solution was  $0.03 \text{ mg}\cdot\text{l}^{-1}$ ; the concentration of ND-Dox and ND-substance 1 varied from  $0.25$  to  $25 \text{ mg}\cdot\text{l}^{-1}$ . Water-alcohol solution of DPPH with the concentration of  $0.03 \text{ mg}\cdot\text{l}^{-1}$  was used as a negative control (without the addition of ND-Dox and ND-substance 1). Water-alcohol dispersions of ND-Dox and ND-substance 1 ( $C = 0.25\text{--}25 \text{ mg}\cdot\text{l}^{-1}$ ) were used as a reference. After preparation the systems were placed in an ultrasonic bath for 10 min and then incubated for 30 min in the dark at  $25^\circ\text{C}$ . Next, the optical density of the solutions was measured relative to the water-alcohol mixture at the wavelength of 515 nm. The degree of inhibition of the free radical reaction was calculated using the equation:

$$\%inhibition = \frac{A_{DPPH} - (A_{mes} - A_0)}{A_{DPPH}} \cdot 100\% \quad (2)$$

where  $A_{DPPH}$  is the optical density of the water-alcohol solution of DPPH in the absence of ND-Dox and ND-substance 1,  $A_{mes}$  is the optical density of the water-alcohol solution of DPPH after the reaction with ND-Dox and ND-substance 1,  $A_0$  is the optical density of the water-alcohol dispersion of ND-Dox and ND-substance 1.

### 2.3.8 Binding with DNA

UV absorption spectra of ND-Dox and ND-substance 1 dispersions in a physiological solution containing DNA in the wavelength range of 220–340 nm were recorded using Thermo Scientific Evolution-300 spectrophotometer (USA) at  $25^\circ\text{C}$  relative to the physiological solution in a quartz cuvette ( $l = 1 \text{ cm}$ ). The solutions were obtained by mixing DNA solutions and dispersions of ND-Dox, ND-substance 1 [34]. The final concentrations of DNA in the dispersions

were 0.0129, 0.0135, 0.0141, 0.0146, 0.0150, 0.0155, 0.0159, 0.0162, 0.0166, 0.0169, and 0.0172 g·l<sup>-1</sup>; the concentrations of ND-Dox and ND-substance 1 were 5·10<sup>-3</sup> g·l<sup>-1</sup>.

### 2.3.9 Effect on the mitochondrial membrane potential ( $\Delta\Psi_m$ )

PANC-1 cells were trypsinised and washed with PBS, containing 10 % fetal bovine serum (FBS). Afterwards, the cells were resuspended in the mixture of PBS, 5 % FBS and 50 mM KCl. After the incubation of the cells with MitoTracker® Orange CMTMRos fluorescent dye (500 nM) at 37 °C for 30 min, they were rinsed with PBS and plated into the black 96-well plate (80,000 cells per well). The concentration of ND, ND-Dox and ND-substance 1 in the final suspensions were equal to 0.075 wt %. For the dissipation of the proton gradient, 10 μM of FCCP (carbonyl cyanide-*p*-trifluoromethoxyphenylhydrazone) were added. The measurements of fluorescence were carried out using the microplate reader (TECAN Instrument, Austria) at the excitation/emission wavelength of 554/576 nm.

## 3. Results

### 3.1 <sup>13</sup>C NMR

Fig. 4 shows the results of <sup>13</sup>C solid-state NMR spectroscopy for ND, substance 1, ND-substance 1 (Fig. 4a) and ND, Dox and ND-Dox (Fig. 4b), respectively. The interpretation of the spectra of substance 1 and Dox is presented in Figs. 4a, b. Moreover, The spectrum of individual ND is shown in Figs. 4a, b for the comparison. It consists of the following shifts: (i) 40 ppm corresponding to the idealised diamond core; (ii) 75 ppm for the hydroxylated carbon atoms; (iii) 100 ppm for the sp<sup>2</sup> carbon atoms covering the ND core due to partial graphitization; (iv) 160, 184 ppm for the surface carbonyl and carboxyl groups. The obtained spectrum is in good agreement with the literature data [36,37]. When comparing the spectra of ND, substance 1 and conjugate, it is obvious, that substance 1 is linked to ND through an ester group (signal at 120 ppm) (Fig. 4a); the signal of the carbon atom in carboxylic group of ND (172 ppm, signal *m*) is shifted towards 182 ppm (signal *b*). Fig. 4b shows that the peak at 172 ppm (*d*) is related to the carbon atom of the amide group formed by the covalent functionalization of the carboxylic group

of ND with amino group of Dox. The rest of the signals in Figs. 4a, b are [the](#) superposition of the peaks of the individual ND and substance 1, Dox.

### 3.2 IR

Fig. 5 shows the IR spectra of ND-substance 1 and ND-Dox, as well as the spectra of precursors for the synthesis of [the](#) conjugates (ND, substance 1, Dox). [The](#) peaks at  $3414\text{ cm}^{-1}$  and  $1630\text{ cm}^{-1}$  correspond to O–H stretching and bending vibrations. [The](#) two peaks at  $2930\text{ cm}^{-1}$  and  $2860\text{ cm}^{-1}$  belong to asymmetric and symmetric C–H stretching vibrations. The peaks at  $1790\text{ cm}^{-1}$  and  $1280\text{ cm}^{-1}$  correspond to the stretching and bending vibrations of the C=O fragments in the lactone and C–O fragments in the epoxy and ester groups. The peak at  $1140\text{ cm}^{-1}$  can be attributed both to [the](#) stretching vibrations of the C–O fragment of the alcohol group and to [the](#) asymmetric bending vibrations of the C–O–C fragment in the composition of the lactol group, ethers, and esters. The spectra of ND–substance 1 and ND–Dox conjugates contain bands characteristic [for](#) both ND and individual cytostatic drugs. The covalent functionalization of ND is confirmed by the presence in the IR spectra of ND-Dox of peaks at  $1645\text{ cm}^{-1}$  and  $1605\text{ cm}^{-1}$ , which are related to C=O stretching vibrations and N–H bending vibrations of the amide bond; and in the case of ND-substance 1, the presence of bands in the region of  $1208\text{--}1000\text{ cm}^{-1}$ , which correspond to the stretching vibrations of the C–O bond in esters.

### 3.3 TEM

Fig. 6 presents [the](#) TEM images of ND, ND–substance 1 и ND–Dox. It can be seen that in the process of functionalization, the layer was formed. The thickness of [the](#) layer is 0.5 nm and [it is](#) unstructured because of organic origin. The cytostatic layer veils the visibility of the ND crystal faceting that is different from the individual ND, which images clearly show their shape and structure even in the presence of the background texture imposed by the underlying carbon film.

### 3.4 Determination of ND-Dox and ND-substance 1 distribution and $\zeta$ -potential

Fig. 7 presents [the](#) size distribution of ND–substance 1 and ND–Dox nanoparticles in aqueous dispersions. The hydrodynamic diameter in aqueous dispersions containing ND-

substance 1, ND-Dox ( $C_{\text{ND-Substance 1/Dox}} = 1 \text{ g}\cdot\text{l}^{-1}$ ) is equal to  $25 \pm 5 \text{ nm}$  and  $30 \pm 5 \text{ nm}$ , respectively (Fig. 7). The Analysis of  $\zeta$ -potentials distribution reveals that the values are in the region  $-36.8 \pm 5 \text{ mV}$  for both conjugates indicating the aggregative stability of the aqueous dispersions in the whole concentration range.

### 3.5 XPS

The XPS spectra of ND-substance 1 and ND-Dox (Figs. 8a, 9a) show C 1s (286 eV), O 1s (532 eV), and N 1s (400 eV) peaks. Figs. 8b, 9b show the result of deconvolution of the C 1s peak with the formation of two peaks at the following binding energies: 285.4 eV (C = C, C-C groups of the ND framework), at 286.5 eV (C – O fragments of epoxy, carbonyl, and hydroxyl groups in the case of the ND-substance 1, ND-Dox conjugate). The 1s oxygen peak consists of the following signals (Fig. 8c, 9c): 532.4 eV, belonging to the O – H groups (Fig. 8c, 9c); 533 eV related to C–O, C=O (epoxy, carbonyl, and hydroxyl groups on the ND surface Fig. 8c, 9c).

### 3.6 Hemocompatibility

#### 3.6.1 Hemolysis

To assess the biocompatibility of ND-Dox and ND-substance 1, its effect on spontaneous hemolysis was studied. The effect of the test substances on hemolysis was determined by measuring the concentration of released hemoglobin. The degree of hemolysis was determined by the formula:

$$\% \text{ haemolysis} = \frac{A_{\text{test}} - A_{\text{control}}}{A_{100}} \cdot 100\% \quad (2)$$

where  $A_{\text{test}}$  is the optical density of the experimental sample;  $A_{\text{control}}$  is the optical density of the control sample;  $A_{100}$  is the optical density of the system with complete hemolysis.

Fig. 10 shows that ND-Dox, when incubated for 1 and 3 h, caused very mild hemolysis (less than 5%) over the entire concentration range; the degree of hemolysis depended on the dose and time. It should be noted that nanomaterials are classified as non-hemolytic if the degree of hemolysis does not exceed 5%. In the case of the dispersions of ND and ND-substance 1, after 1

and 3 h of incubation, hemolysis was not observed in the studied concentration range 0.075–0.3 g·l<sup>-1</sup>. Therefore, ND-substance 1 and ND-Dox can be considered safe in the concentration range up to 0.3 g·l<sup>-1</sup>.

### 3.6.2 Platelet aggregation

It was found (Table 2) that ND at all studied concentrations did not affect ADP-induced platelet aggregation, and in the tests of collagen- and adrenaline-induced aggregation, there was a significant suppression of aggregation compared to the control only at the maximum concentration of 0.3 g·l<sup>-1</sup>. The ND-Dox conjugate statistically significantly inhibited adrenaline- and ADP-induced platelet aggregation compared to the control and did not affect collagen-induced platelet aggregation. The ND-substance 1 conjugate significantly inhibited ADP-, collagen-, and adrenaline-induced platelet aggregation only at the maximum concentration of 0.3 g·l<sup>-1</sup> compared to the control.

### 3.6.3 Clotting test

The effect of ND, ND-Dox and ND-substance 1 on the parameters of the plasma-coagulation hemostasis is presented in Table 3. As can be seen from the presented data, there was a statistically significant increase in PT compared to the control only at the maximum concentration of ND-Dox and ND-substance 1 (0.3 g·l<sup>-1</sup>). ND-substance 1 statistically significantly reduced TT at the concentrations of 0.075–0.3 g·l<sup>-1</sup>. In the studied concentration range, ND, ND-Dox and ND-substance 1 did not affect aPTT.

### 3.6.4 Binding with HSA

The Scatchard equation was used to determine the binding constant ( $K_b$ ) of ND-Dox and ND-substance 1 to HSA from fluorescence spectroscopy data:

$$\lg \frac{F_0 - F}{F} = \lg K_b + n \lg Q \quad (1);$$

where  $F_0$  is HSA fluorescence intensity in the absence of nanomaterials,  $F$  is HSA fluorescence intensity in the presence of the nanomaterials,  $Q$  is the concentration of the nanomaterial, g·l<sup>-1</sup>.

Fig. 11 shows the data on HSA binding to ND-Dox and ND-substance 1 in Hill coordinates ( $\lg \frac{F_0 - F}{F}$ ,  $\lg Q$ ).

To determine the binding sites of ND-Dox and ND-substance 1 with HSA, competitive binding experiments were performed in the presence of binding site markers. The measurements were carried out in the absence and in the presence of binding site markers, which were used as warfarin, ibuprofen, and digitonin with the final concentration of  $C = 3 \mu\text{M}$ . The calculations were carried out based on three parallel measurements.

From the data obtained for ND-substance 1, the  $K_b$  and  $n$  values decreased in the presence of ibuprofen and digitonin (Table 4), and in the case of ND-Dox, in the presence of ibuprofen, digitonin, and warfarin (Table 5). Based on the values of the binding constants, ND-Dox forms a stronger complex with HSA in the IIIA subdomain and less stable complexes in the IB, IIA subdomains; ND-substance 1 forms a stronger complex with HSA in the IIIA subdomain and a weaker complex in the IB subdomain.

### 3.6.5 Antiradical activity

Fig. 12 and 13 show the dependence of the fraction of reduced radicals (% inhibition) on the concentration of ND-Dox and ND-substance 1. From Fig. 12 and 13, we can conclude that the antiradical activity of ND-Dox and ND-substance 1 increases with increasing concentration ( $C = 0.25\text{--}25 \text{ mg}\cdot\text{l}^{-1}$ ). It is impossible to determine the  $IC_{50}$  value (sample concentration required to achieve 50% inhibition) of the DPPH radical for ND-Dox conjugate, since inhibition is less than 50% in the studied concentration range (Fig. 12), while for ND-substance 1  $IC_{50}$  is  $12.5 \text{ mg}\cdot\text{l}^{-1}$  (Fig. 13). For comparison, we can cite the data on the antiradical activity of the ND dispersion: the maximum percentage of inhibition was 37.9% at the nanoparticle concentration of  $200 \text{ mg}\cdot\text{l}^{-1}$ . The ND-substance 1 derivative exhibits significant antiradical activity as compared to ND and ND-Dox, which may be related to surface functionalization. Substance 1 was also shown to be able to scavenge free radicals in a model reaction with DPPH ( $k(303.15 \text{ K}) = (2.43 \pm 0.06) \cdot 10^{-3} \text{ min}^{-1}$ ) [34].



### 3.6.6 Cytotoxicity and study of the mechanisms of endocytosis

Analysis of the obtained data shows that in the presence of the CK-636 inhibitor, the survival of HeLa cells increases in the presence of the ND-substance 1 conjugate. The regulation of rearrangements of the actin cytoskeleton is important for processes such as cell movement, endocytosis, and intracellular movement of lipid vesicles. Therefore, the ND-substance 1 conjugate is transported into cells by actin-dependent endocytosis (Fig. 14).

In the case of the ND-Dox conjugate, the survival of the HeLa cell line is increased in the presence of CK-636 and Clorpronazine, which is an inhibitor of the clathrin-dependent endocytosis. Thus, it can be assumed that the ND-Dox conjugate is transported into cells mainly by actin- and clathrin-dependent endocytosis (Fig. 14b).

The analysis of Table 6 and Fig. 15 allows to conclude the following:

(i) individual ND has no cytotoxic effect on PANC-1, T98G, HeLa cell lines in the concentration range up to  $0.15 \text{ g}\cdot\text{l}^{-1}$ ;

(ii) the analysis of  $IC_{50}$  values shows that the cytotoxic effect of ND-Dox and ND-substance 1 conjugates is comparable to the effect of individual cytostatic drugs (Dox and substance 1);

(iii) the highest cytotoxic effect is observed for the ND-substance 1 conjugate on the T98G cell line, while the effectiveness of the ND-substance 1 conjugate is 15 times higher than the effect of individual substance 1 and 175 times higher than the effect of individual Dox.

### 3.6.7 Binding with DNA

Fig. 16 shows the absorption spectra of a DNA solution, the dispersion containing DNA and ND-Dox, DNA and ND-substance 1. It can be seen that the addition of ND-Dox and ND-substance 1 to DNA leads to a strong hyperchromic effect, while there is no shift in the absorption maximum of DNA. It should be noted that in the studied range of concentrations, the linear dependence in Wulf-Shimmer coordinates for ND-Dox and ND-substance 1 is observed (Fig. 17).

Hyperchromism is explained by the presence of synergistic non-covalent interactions of ND-Dox and ND-substance with DNA, namely electrostatic interactions, hydrogen bonding, and binding to the DNA surface. Since there is no change in the position of the absorption bands (bathochromic or hypsochromic shifts), it can be concluded that ND-Dox and ND-substance binds non-covalently to the DNA molecule.

Binding constants ( $k_{bin}$ ) were calculated using the Wolfe–Shimmer equation:

$$\frac{[DNA]}{\varepsilon_a - \varepsilon_f} = \frac{[DNA]}{\varepsilon_b - \varepsilon_f} + \frac{1}{k_{bin}(\varepsilon_b - \varepsilon_f)} \quad (3)$$

where [DNA] is the concentration of DNA,  $\varepsilon_a$ ,  $\varepsilon_f$ ,  $\varepsilon_b$  are the extinction coefficient of the ND-Dox and ND-substance 1 with DNA, the extinction coefficient for free ND-Dox and ND-substance 1 and the extinction coefficient for ND-Dox and ND-substance 1 in fully bound form respectively.

As a result, the following values of the binding constants of the studied conjugate with DNA were obtained:  $k_{bin} = (520.5 \pm 45.7) \cdot 10^{-3} \text{ l} \cdot \text{mg}^{-1}$  (DNA-ND-Dox),  $k_{bin} = (389.0 \pm 60.1) \cdot 10^{-3} \text{ l} \cdot \text{mg}^{-1}$  (DNA- ND-substance 1).

### 3.6.8 Effect on the mitochondrial membrane potential ( $\Delta\Psi_m$ )

The results of the effect of ND-Dox and ND-substance 1 conjugates on the fluorescence intensity of the MitoTracker® Orange CTMMRos probe is shown in Fig. 18.

As can be seen from the presented data, the addition of ND-Dox and ND-substance 1 decreased  $\Delta\Psi_m$ : the fluorescence intensity in relation to the control (100.0±22.0%) was 30.4±4.6%, 6.9 ±0.9% and 27.9±5.1, respectively. The most significant effect was noted for ND-Dox (6.9±0.9%). For ND and ND-substance 1, comparable results were obtained (30.4±4.6% and 27.9±5.1%).

Compared to ND-Dox, Dox had a smaller effect on the value of  $\Delta\Psi_m$ : (the fluorescence intensity relative to the control was 52.2±7.1%), and substance 1 practically did not cause any fluorescence (83.1±13.8%).

In an-the experiment on the effect on the mitochondrial membrane potential, ND–Dox conjugates reduced the membrane potential significantly more than ND or Dox (6.9±0.9%,

30.4±4.6%, and 52.2±7.1%, respectively). Apparently, this is due to the formation of a binary effect, i.e., a-the combination of the uncoupling effect of ND and Dox-dependent generation of reactive oxygen species.

In the present study the ability of Dox to reduce the level of mitochondrial membrane potential was found, without affecting the activity of ATPase.

Taking into account that substance 1 had practically no effect on the value of the membrane mitochondrial potential (83.1±13.8%) and comparable results obtained by us for ND and ND-Diox (30.4±4.6% and 27.9±5.1 %, respectively), it can be assumed that the decrease in the mitochondrial membrane potential upon the addition of ND-substance 1 is due only to the uncoupling effect of ND.

### Conclusions

We present new experimental data on the synthesis and characterization of covalent conjugates based on ND, substance 1, and Dox. The study of biocompatibility and biological activity of ND-Dox and ND-substance 1 allows to conclude the following: (i) ND-Dox and ND-substance 1 interact with HSA, forming a complex in IIIA subdomain of HSA; (ii) ND-substance 1 exhibits antiradical activity (based on the data from the study of a model reaction with DPPH); (iii) the ND-Dox and ND-substance 1 conjugates are hemocompatible (based on the data on hemolysis, the study of parameters of plasma-coagulation hemostasis, as well as the platelet aggregation); (iv) they interact with the DNA molecule (ND-Dox:  $k_{bin} = (520.5 \pm 45.7) \cdot 10^{-3} \text{ l} \cdot \text{mg}^{-1}$ , ND-substance 1 with DNA  $k_{bin} = (389.0 \pm 60.1) \cdot 10^{-3} \text{ l} \cdot \text{mg}^{-1}$ ); (v) the highest cytotoxic effect is observed for the ND-substance 1 conjugate on the T98G cell line, while the effectiveness of the ND-substance 1 conjugate is 15 times higher than the effect of the individual substance 1 and 175 times higher than the effect of the individual Dox; (vi) ND-substance 1 conjugate is transported into cells by actin-dependent endocytosis and ND-Dox demonstrate both actin- and clathrin-dependent endocytosis

### Acknowledgements

The research was performed using the equipment of the Center for optical and laser materials research, Research Centre for X-ray diffraction studies, Magnetic Resonance Research Center, Center for Physical methods of surface investigation, Thermogravimetric and Calorimetric Research Center, Computer Center of SPbU and the Centre for Chemical analysis and materials research of the Research Park of Saint Petersburg State University.

## References

- [1] F. Cataldo, T. Da Ros, Medicinal chemistry and pharmacological potential of fullerenes and carbon nanotubes, Springer, 2008.
- [2] S. V. Eswaran, Water Soluble Nanocarbon Materials:A Panacea for All?, *Curr. Sci.* 114 (2018) 1846–1850. <https://doi.org/10.18520/CS/V114/I09/1846-1850>.
- [3] M. De Sousa, L.A. Visani De Luna, L.C. Fonseca, S. Giorgio, O.L. Alves, Folic-Acid-Functionalized Graphene Oxide Nanocarrier: Synthetic Approaches, Characterization, Drug Delivery Study, and Antitumor Screening, *ACS Appl. Nano Mater.* 1 (2018) 922–932. <https://doi.org/10.1021/acsanm.7b00324>.
- [4] V. Biju, Chemical modifications and bioconjugate reactions of nanomaterials for sensing, imaging, drug delivery and therapy, *Chem. Soc. Rev.* 43 (2014) 744–764. <https://doi.org/10.1039/c3cs60273g>.
- [5] Amnon Bar-Shir, and Yoni Engel, M. Gozin\*, Synthesis and Water Solubility of Adamantyl-OEG-fullerene Hybrids, (2005). <https://doi.org/10.1021/JO0479359>.
- [6] X. Fu, Y. Shi, T. Qi, S. Qiu, Y. Huang, X. Zhao, Q. Sun, G. Lin, Precise design strategies of nanomedicine for improving cancer therapeutic efficacy using subcellular targeting, *Signal Transduct. Target. Ther.* 5 (2020) 262. <https://doi.org/10.1038/s41392-020-00342-0>.
- [7] I.N. Gaponenko, S. V. Ageev, G.O. Iurev, O.S. Shemchuk, A.A. Meshcheriakov, A. V. Petrov, I.L. Solovtsova, L. V. Vasina, T.B. Tennikova, I. V. Murin, K.N. Semenov, V. V. Sharoyko, Biological evaluation and molecular dynamics simulation of water-soluble fullerene derivative C60[C(COOH)2]3, *Toxicol. Vitri.* 62 (2020) 104683. <https://doi.org/10.1016/j.tiv.2019.104683>.
- [8] V. V. Sharoyko, O.S. Shemchuk, A.A. Meshcheriakov, L. V. Vasina, N.R. Iamalova, M.D. Luttsev, D.A. Ivanova, A. V. Petrov, D.N. Maystrenko, O.E. Molchanov, K.N. Semenov, Biocompatibility, antioxidant activity and collagen photoprotection properties of C60

- fullerene adduct with L-methionine, *Nanomedicine Nanotechnology, Biol. Med.* 40 (2022) 102500. <https://doi.org/10.1016/J.NANO.2021.102500>.
- [9] Z. Hussain, I. Ullah, Z. Wang, P. Ding, S. Ullah, Y. Zhang, Z. Zhang, J. Yan, B. Luo, R. Pei, Electrospun nanofibrous membrane functionalized with dual drug-cyclodextrin inclusion complexes for the potential treatment of otitis externa, *Colloids Surfaces A Physicochem. Eng. Asp.* 651 (2022) 129742. <https://doi.org/10.1016/j.colsurfa.2022.129742>.
- [10] V. De Leo, A.M. Maurelli, L. Giotta, L. Catucci, Liposomes containing nanoparticles: preparation and applications, *Colloids Surfaces B Biointerfaces.* 218 (2022) 112737. <https://doi.org/10.1016/j.colsurfb.2022.112737>.
- [11] H. Manoochehri, A. Jalali, H. Tanzadehpanah, A. Taherkhani, R. Najafi, Aptamer-conjugated nanoliposomes containing COL1A1 siRNA sensitize CRC cells to conventional chemotherapeutic drugs, *Colloids Surfaces B Biointerfaces.* 218 (2022) 112714. <https://doi.org/10.1016/j.colsurfb.2022.112714>.
- [12] Q. Zhao, P. Xie, X. Li, Y. Wang, Y. Zhang, S. Wang, Magnetic mesoporous silica nanoparticles mediated redox and pH dual-responsive target drug delivery for combined magnetothermal therapy and chemotherapy, *Colloids Surfaces A Physicochem. Eng. Asp.* 648 (2022) 129359. <https://doi.org/10.1016/j.colsurfa.2022.129359>.
- [13] X. Gong, Z. Wang, L. Zhang, W. Dong, R. Wang, Y. Liu, S. Song, Q. Hu, F. Du, S. Shuang, C. Dong, A novel carbon-nanodots-based theranostic nano-drug delivery system for mitochondria-targeted imaging and glutathione-activated delivering camptothecin, *Colloids Surfaces B Biointerfaces.* 218 (2022) 112712. <https://doi.org/10.1016/j.colsurfb.2022.112712>.
- [14] Z. Jiang, J. He, X. Wang, D. Zhu, N. Li, L. Ren, G. Yang, Nanomaterial-based cell sheet technology for regenerative medicine and tissue engineering, *Colloids Surfaces B Biointerfaces.* 217 (2022) 112661. <https://doi.org/10.1016/j.colsurfb.2022.112661>.

- [15] C. Auría-Soro, T. Nesma, P. Juanes-Velasco, A. Landeira-Viñuela, H. Fidalgo-Gomez, V. Acebes-Fernandez, R. Gongora, M.J. Almendral Parra, R. Manzano-Roman, M. Fuentes, Interactions of Nanoparticles and Biosystems: Microenvironment of Nanoparticles and Biomolecules in Nanomedicine, *Nanomaterials*. 9 (2019) 1365. <https://doi.org/10.3390/nano9101365>.
- [16] B. AS, Diamond standard in diagnostics: nanodiamond biolabels make their mark, *Analyst*. 134 (2009) 1751–1764. <https://doi.org/10.1039/B908532G>.
- [17] K. van der Laan, M. Hasani, T. Zheng, R. Schirhagl, Nanodiamonds for In Vivo Applications, *Small*. 14 (2018) 1703838. <https://doi.org/10.1002/sml.201703838>.
- [18] Y.Y. Hui, C.-L. Cheng, H.-C. Chang, Nanodiamonds for optical bioimaging, *J. Phys. D: Appl. Phys.* 43 (2010) 374021. <https://doi.org/10.1088/0022-3727/43/37/374021>.
- [19] X. Y, D. L, Nanodiamonds for nanomedicine, *Nanomedicine (Lond)*. 4 (2009) 207–218. <https://doi.org/10.2217/17435889.4.2.207>.
- [20] K.A. Mitura, E. Włodarczyk, Fluorescent Nanodiamonds in Biomedical Applications, *J. AOAC Int*. 101 (2018) 1297–1307. <https://doi.org/10.5740/jaoacint.18-0044>.
- [21] H. Tinwala, S. Wairkar, Production, surface modification and biomedical applications of nanodiamonds: A sparkling tool for theranostics, *Mater. Sci. Eng. C*. 97 (2019) 913–931. <https://doi.org/10.1016/j.msec.2018.12.073>.
- [22] L. Zhang, G. Feng, W. Zhou, Y. Zhang, L. Wang, L. Wang, Z. Liu, T. Zhao, W. Zhu, B. Zhang, Core-shell sp<sup>3</sup>@sp<sup>2</sup> nanocarbon for adsorption of anionic and cationic organic dyes: Effect of the graphitization of nanocarbon, *Colloids Surfaces A Physicochem. Eng. Asp*. 651 (2022) 129694. <https://doi.org/10.1016/j.colsurfa.2022.129694>.
- [23] N. Bondon, L. Raehm, C. Charnay, R. Boukherroub, J.-O. Durand, Nanodiamonds for bioapplications, recent developments, *J. Mater. Chem. B*. 8 (2020) 10878–10896. <https://doi.org/10.1039/D0TB02221G>.
- [24] N. Panwar, A.M. Soehartono, K.K. Chan, S. Zeng, G. Xu, J. Qu, P. Coquet, K.-T. Yong, X.

- Chen, Nanocarbons for Biology and Medicine: Sensing, Imaging, and Drug Delivery, *Chem. Rev.* 119 (2019) 9559–9656. <https://doi.org/10.1021/acs.chemrev.9b00099>.
- [25] M.S. Ali, A.A. Metwally, R.H. Fahmy, R. Osman, Nanodiamonds: Minuscule gems that ferry antineoplastic drugs to resistant tumors, *Int. J. Pharm.* 558 (2019) 165–176. <https://doi.org/10.1016/j.ijpharm.2018.12.090>.
- [26] L.P. Suarez-Kelly, A.R. Campbell, I. V. Rampersaud, A. Bumb, M.S. Wang, J.P. Butchar, S. Tridandapani, L. Yu, A.A. Rampersaud, W.E. Carson, Fluorescent nanodiamonds engage innate immune effector cells: A potential vehicle for targeted anti-tumor immunotherapy, *Nanomedicine Nanotechnology, Biol. Med.* 13 (2017) 909–920. <https://doi.org/10.1016/j.nano.2016.12.005>.
- [27] Y. Octavia, C.G. Tocchetti, K.L. Gabrielson, S. Janssens, H.J. Crijns, A.L. Moens, Doxorubicin-induced cardiomyopathy: From molecular mechanisms to therapeutic strategies, *J. Mol. Cell. Cardiol.* 52 (2012) 1213–1225. <https://doi.org/10.1016/j.yjmcc.2012.03.006>.
- [28] K.O. Alfarouk, C.M. Stock, S. Taylor, M. Walsh, A.K. Muddathir, D. Verduzco, A.H.H. Bashir, O.Y. Mohammed, G.O. Elhassan, S. Harguindey, S.J. Reshkin, M.E. Ibrahim, C. Rauch, Resistance to cancer chemotherapy: Failure in drug response from ADME to P-gp, *Cancer Cell Int.* 15 (2015) 71. <https://doi.org/10.1186/s12935-015-0221-1>.
- [29] K. Burger, K. Nooter, Cell Cycle Pharmacokinetic Resistance to Imatinib Mesylate: Role of the ABC Drug Pumps ABCG2 (BCRP) and ABCB1 (MDR1) in the Oral Bioavailability of Imatinib, (n.d.). <https://doi.org/10.4161/cc.3.12.1331>.
- [30] F. Lévi, Chronotherapeutics: The relevance of timing in cancer therapy, *Cancer Causes Control.* 17 (2006) 611–621. <https://doi.org/10.1007/s10552-005-9004-7>.
- [31] D.M. Townsend, K.D. Tew, The role of glutathione-S-transferase in anti-cancer drug resistance, *Oncogene.* 22 (2003) 7369–7375. <https://doi.org/10.1038/sj.onc.1206940>.
- [32] M.A. Harkey, M. Czerwinski, J. Slattey, H.-P. Kiem, Overexpression of glutathione-S-



transferase, MGSTII, confers resistance to busulfan and melphalan., *Cancer Invest.* 23 (2005) 19–25.

- [33] O. V Mikolaichuk, E.A. Popova, A. V Protas, I.T. Rakipov, D.A. Nerukh, A. V Petrov, N.A. Charykov, S. V Ageev, G. V Tochilnikov, I.G. Zmitrichenko, A.N. Stukov, K.N. Semenov, V. V Sharoyko, A cytostatic drug from the class of triazine derivatives: Its properties in aqueous solutions, cytotoxicity, and therapeutic activity, *J. Mol. Liq.* 356 (2022) 119043. <https://doi.org/https://doi.org/10.1016/j.molliq.2022.119043>.
- [34] O. V. Mikolaichuk, V. V. Sharoyko, E.A. Popova, A. V. Protas, A. V. Fonin, L. V. Vasina, Y.A. Anufrikov, M.D. Luttsev, I.A. Nashchekina, A.M. Malkova, G. V. Tochilnikov, S. V. Ageev, K.N. Semenov, Biocompatibility and bioactivity study of a cytostatic drug belonging to the group of alkylating agents of the triazine derivative class, *J. Mol. Liq.* 343 (2021) 117630. <https://doi.org/10.1016/j.molliq.2021.117630>.
- [35] M. Gershanovich, V. Filov, Results of a cooperative clinical study of the anticancer drug dioxadet in phase II, *Vopr Oncol.* 44 (1998) 216–220.
- [36] G.M. Berdichevskiy, L. V. Vasina, S. V. Ageev, A.A. Meshcheriakov, M.A. Galkin, R.R. Ishmukhametov, A. V. Nashchekin, D.A. Kirilenko, A. V. Petrov, S.D. Martynova, K.N. Semenov, V. V. Sharoyko, A comprehensive study of biocompatibility of detonation nanodiamonds, *J. Mol. Liq.* 332 (2021). <https://doi.org/10.1016/j.molliq.2021.115763>.
- [37] A.S. Mazur, M.A. Vovk, P.M. Tolstoy, Solid-state <sup>13</sup>C NMR of carbon nanostructures (milled graphite, graphene, carbon nanotubes, nanodiamonds, fullerenes) in 2000–2019: a mini-review, *Fullerenes Nanotub. Carbon Nanostructures.* 28 (2020) 202–213. <https://doi.org/10.1080/1536383X.2019.1686622>.

Table 1. Reagents used in the study

№	Sample	Manufacturer	Main substance content
1	Sodium nitrate	Vekton, Russia	$\geq 0.95$
2	Potassium permanganate	Vekton, Russia	$\geq 0.99$
3	Sodium hydroxide	Vekton, Russia	$\geq 0.99$
4	L-glutamine	Sigma-Aldrich, USA	$\geq 0.98$
5	HSA	Biolot, Russia	$\geq 0.95$
6	Phosphate-buffered saline	Biolot, Russia	
7	Radachlorin	Rada-Pharma, Russia	
8	Dimethyl sulfoxide	Vekton, Russia	$\geq 0.99$
9	Sodium azide	Sigma-Aldrich, USA	$\geq 0.99$
10	Adenosine diphosphate	Sigma-Aldrich, USA	$\geq 0.95$
11	Sodium citrate	Vekton, Russia	$\geq 0.99$
12	Propidium iodide	Sigma-Aldrich, USA	$\geq 0.94$
13	Hydrogen peroxide	Vekton, Russia	$\geq 0.33$
14	Digitonin	J&K Scientific GmbH, China	$\geq 0.92$
15	Ibuprofen	J&K Scientific GmbH, China	$\geq 0.98$
16	Warfarin	Sigma-Aldrich, USA	$\geq 0.97$

Table 2. Influence on ADP, collagen, adrenaline - induced platelet aggregation in platelet-rich plasma;  $C_{NM}$  is the concentration of nanomaterials.

Inductor ( $n=7$ )	Amplitude / %			
	$C_{NM} / \text{g} \cdot \text{l}^{-1}$			
	Control	0.075	0.15	0.3
	ND			
ADP	69.4±6.7	73.2±9.5	67.4±8.6	65.0±5.0
Adrenaline	66.5±4.9	63.0±4.7	57.8±5.7	47.8±7.9*
Collagen	79.9±5.2	78.7±8.6	74.5±8.3	65.2±6.8*
	ND-Dox			
	Control	0.075	0.15	0.3
ADP	83.4±6.9	78.3±8.6	72.0±2.9	69.7±4.6*
Adrenaline	80.7±5.3	70.7±5.9*	69.9±7.7*	69.2±7.7*
Collagen	83.2±4.6	78.8±2.7	76.5±4.6	76.4±7.1
	ND-substance 1			
	Control	0.075	0.15	0.3
ADP	80.8±2.6	80.0±5.9	77.5±8.2	73.3±3.2*
Adrenaline	74.0±8.4	78.4±8.1	68.1±9.0	63.2±4.2*
Collagen	85.0±5.6	82.5±4.7	78.3±8.8	75.6±3.3*

\* $p < 0.05$  relative to control

Table 3. Effect of ND-Dox and ND-substance 1 on ADP-, collagen- and adrenaline-induced platelet aggregation in platelet-rich plasma.

	$C / g^{-1}$			
	Control	0.375	0.75	1.5
	<b>PT / s</b>			
ND	14.9±0.9	12.5±1.2	12.0±1.0	12.6±1.1
ND-Dox	13.7±2.1	13.3±1.1	15.2±1.2	21.8±1.6*
ND-substance 1	13.4±1.0	13.4±1.7	13.9±1.0	17.8±1.8*
	<b>aPTT / s</b>			
ND	36.6±0.6	37.3±1.3	38.5±2.0	39.1±1.8
ND-Dox	36.1±1.7	37.33±0.7	38.0±0.9	39.5±1.2
ND-substance 1	36.8±1.1	38.0±0.9	38.3±1.2	36.9±1.2
	<b>TT / s</b>			
ND	17.5±0.9	16.5±2.0	14.4±1.6	14.0±1.5
ND-Dox	15.4±1.2	15.9±0.7	14.7±0.8	12.2±0.6
ND-substance 1	17.5±1.2	16.0±0.9	11.1±1.1*	8.33±0.7*

\* $p < 0.05$  relative to control

Table 4. The values of binding constants ( $K_b$ ) and the stoichiometry of the binding reaction ( $n$ ) ND-substance 1.

ND-substance 1		
Binding marker	$K_b \cdot 10^2 / \text{l} \cdot \text{g}^{-1}$	$n$
–	$17.9 \pm 0.6$	$1.2 \pm 0.3$
Warfarin	$20.1 \pm 0.7$	$1.3 \pm 0.1$
Ibuprofen	$0.3 \pm 0.1$	$1.1 \pm 0.1$
Digitonin	$9.9 \pm 0.4$	$1.2 \pm 0.2$

Table 5. The values of binding constants ( $K_b$ ) and the stoichiometry of the binding reaction ( $n$ ) ND-Dox.

ND-Dox		
Binding marker	$K_b \cdot 10^2, l \cdot g^{-1}$	$n$
–	$9.7 \pm 0.5$	$0.5 \pm 0.1$
Warfarin	$1.7 \pm 0.4$	$0.3 \pm 0.1$
Ibuprofen	$0.1 \pm 0.1$	$0.4 \pm 0.1$
Digitonin	$1.1 \pm 0.1$	$0.4 \pm 0.1$

Table 6.  $IC_{50}$  values for cell lines Panc-1, T98G and HeLa for ND, ND-Dox and ND-substance 1, as well as individual Dox and substance 1. In parentheses are the concentrations in terms of individual substances Dox and substance 1.

Substance	$IC_{50}$		
	PANC-1	T98G	HeLa
ND / $mg \cdot l^{-1}$	-	-	-
ND-Dox / $mg \cdot l^{-1}$	24.0±1.2 (37.0±2.0 $\mu M$ )	1.4±0.1 (2.2±1.1 $\mu M$ )	2.2±0.1 (2.8±0.1 $\mu M$ )
ND-Substance 1 / $mg \cdot l^{-1}$	53.0±3.27 (112±6 $\mu M$ )	0.09±0.01 (0.20±0.01 $\mu M$ )	2.9±0.2 (6.2±0.3 $\mu M$ )
Dox / $\mu M$	0.30±0.02	35.0±1.8	2.3±0.1
Substance 1 / $\mu M$	33.3±1.7	3.0±0.2	5.0±0.3

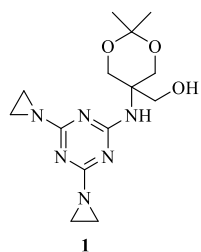


Fig. 1 The structure of substance 1



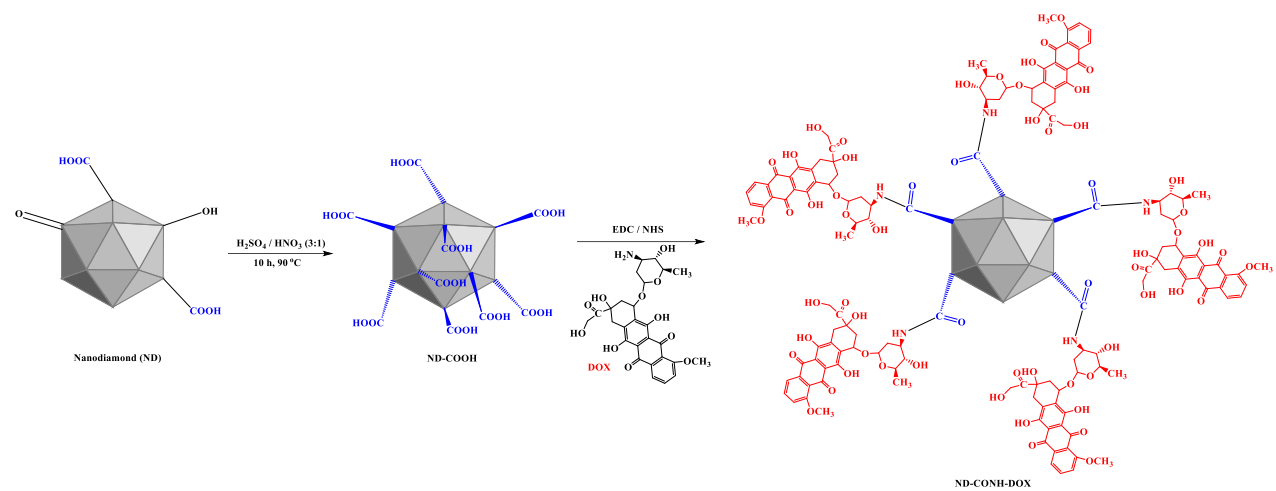


Fig. 2 The synthesis of ND covalently functionalized with DOX (ND-CONH-DOX) through amidation reaction.

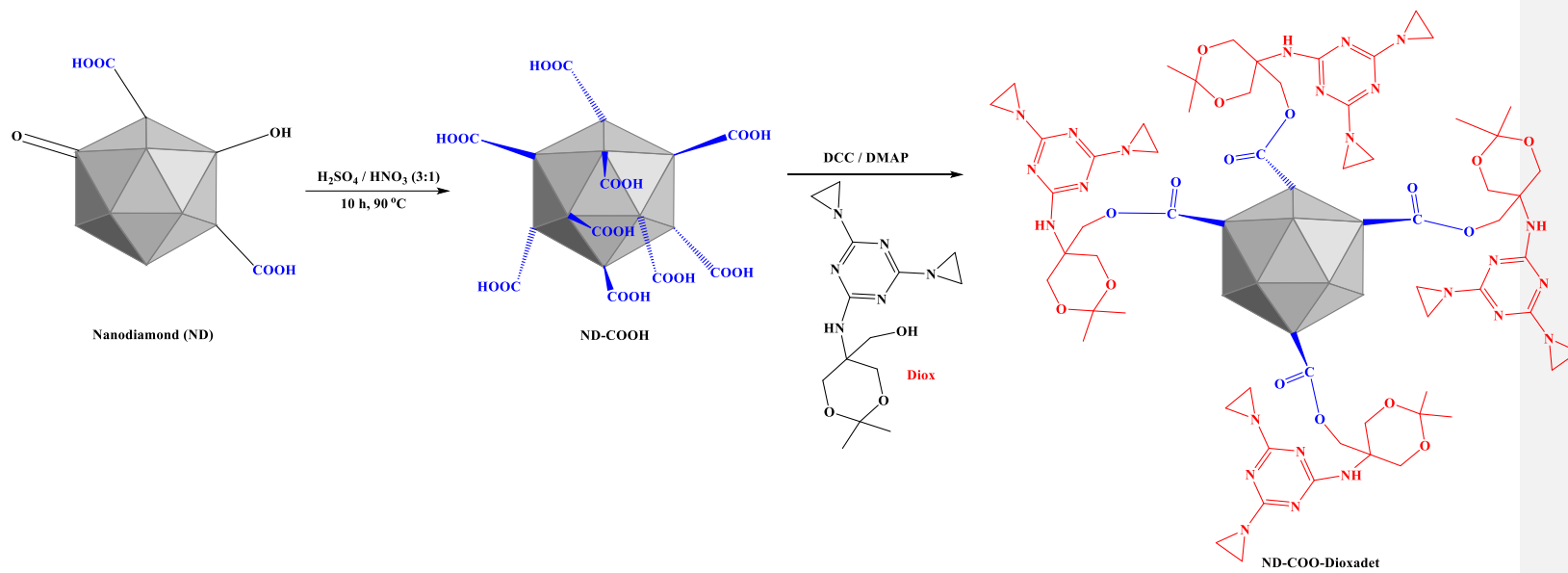
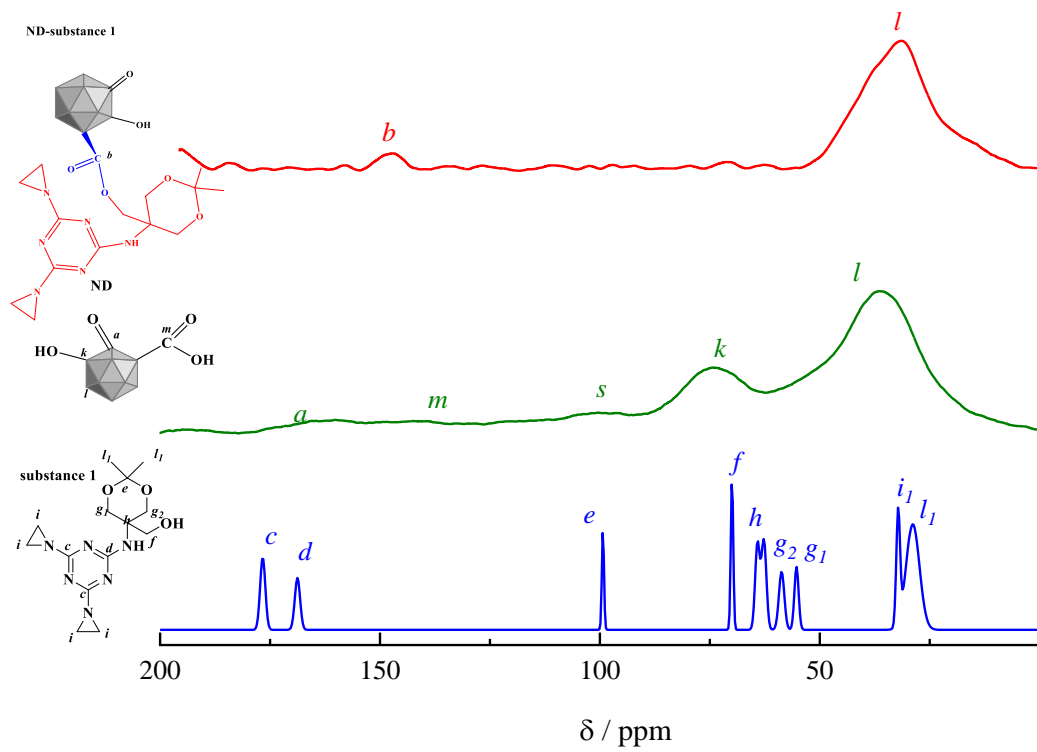


Fig. 3 The synthesis of ND covalently functionalised with substance 1 (ND-COO-substance 1) through esterification reaction.

(a)



(b)

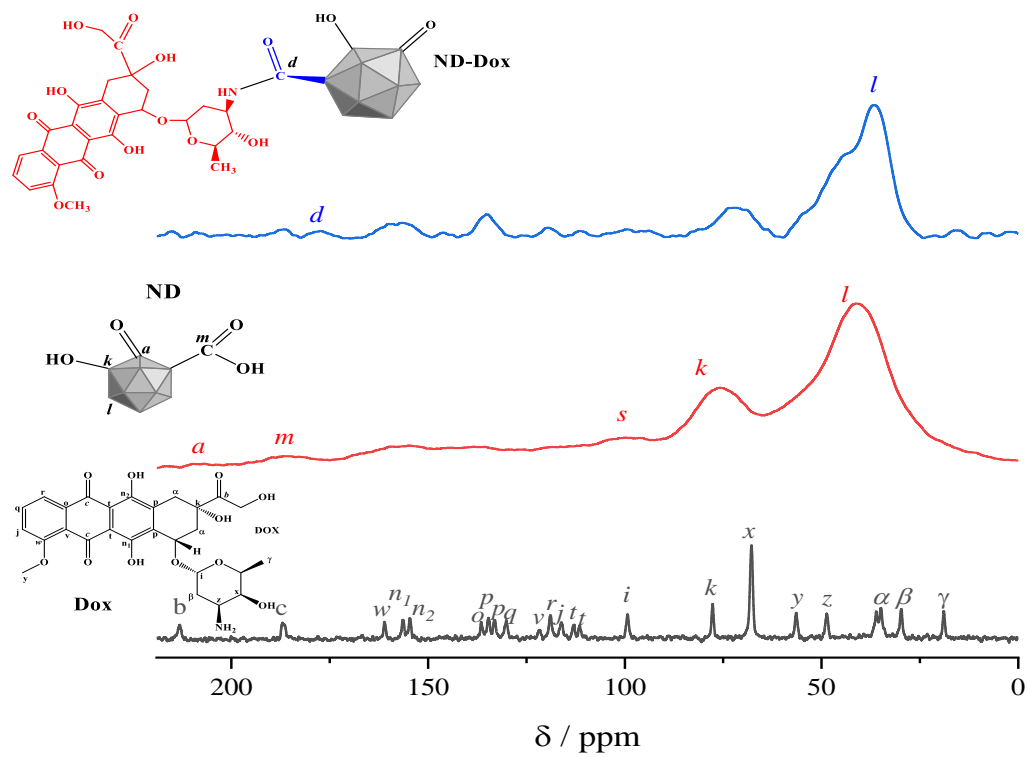
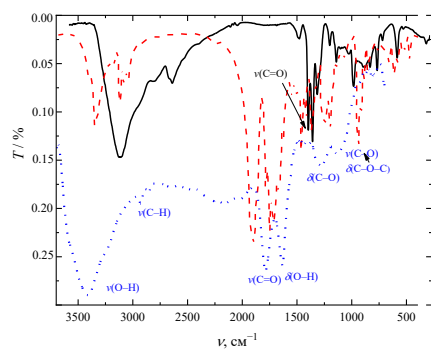


Fig. 4 <sup>13</sup>C NMR spectra of ND-substance 1 (●), ND (●), substance 1 (●) (a) and ND-Dox (●), ND (●), Dox (●) (b).

(a)



(b)

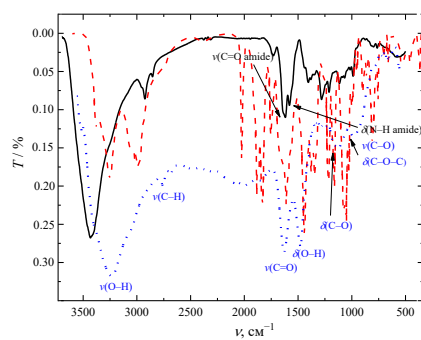


Fig 5. IR-spectra of (a) ND-substance 1 (black), substance 1 (red) и ND (blue); (b) ND-Dox (black), Dox (red) и ND (blue).

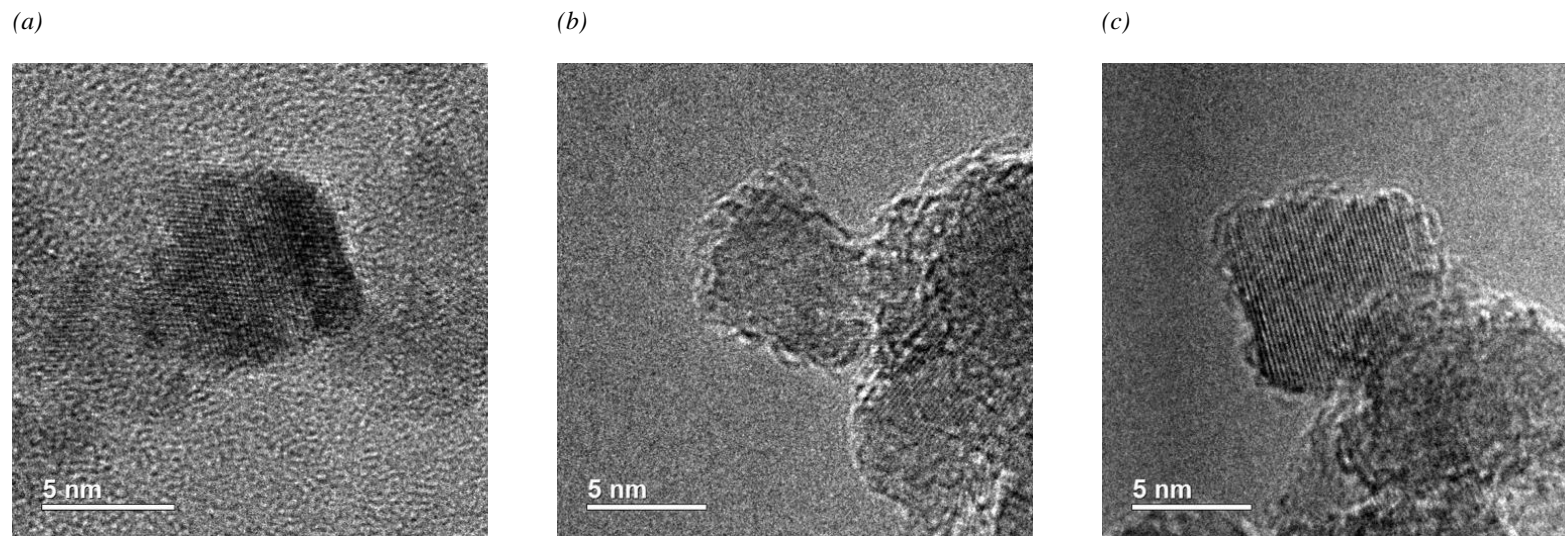
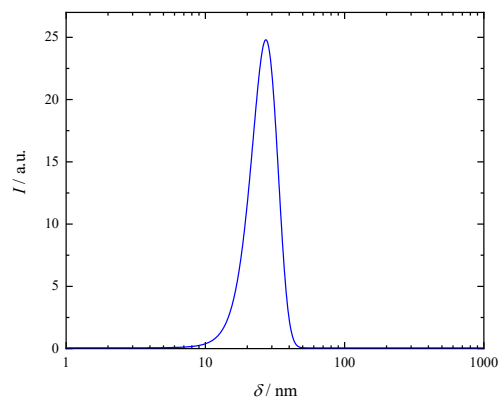


Fig. 6. A-characteristic Typical TEM-images of a individual ND (a), ND-substance 1 (b), and ND-Dox (c)

(a)



(b)

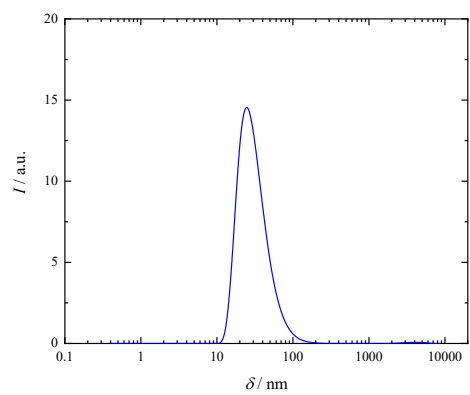
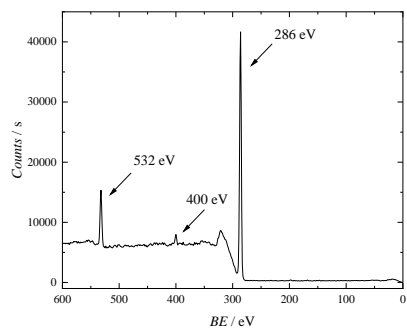


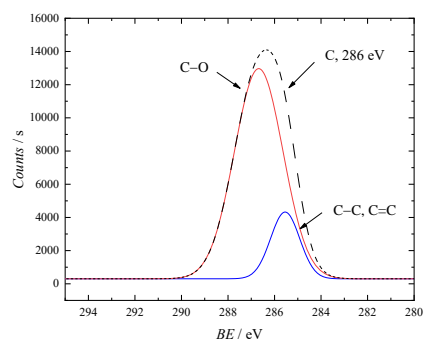
Fig. 7 The size distribution of the nanoparticles of ND-substance 1 (a) and ND-Dox (b) ( $C=1 \text{ g}\cdot\text{l}^{-1}$ )

1)

(a)



(b)



(c)

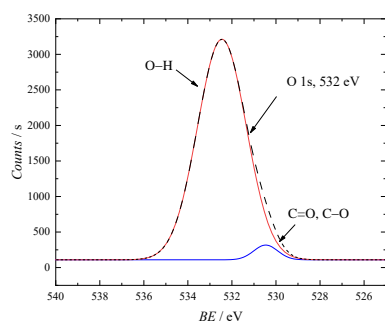


Fig. 8 XPS spectra of ND-substance 1 (a), C 1s (b) and O 1s (c) peak deconvolution.



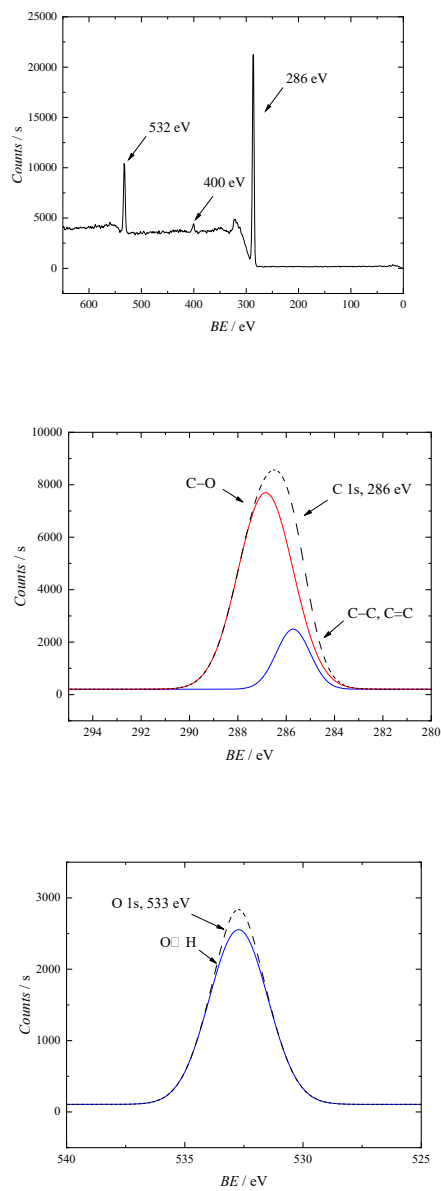


Fig. 9 XPS spectra ND-Dox (a), C 1s (b) и O 1s (c) peaks deconvolution.

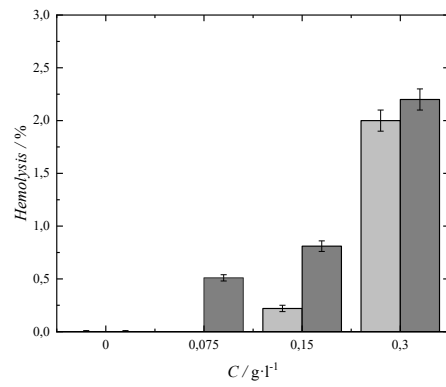
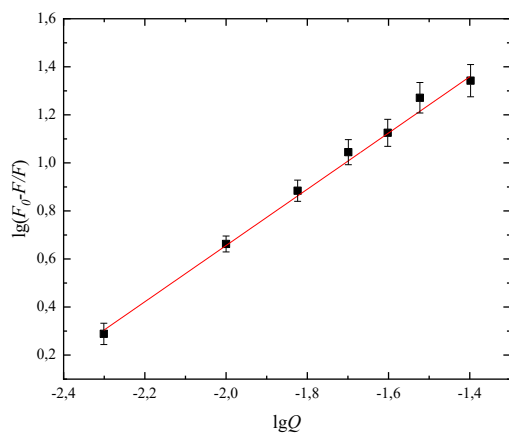


Fig. 10. **The** effect of ND-Dox on the degree of hemolysis of erythrocytes after 1 h (light gray) and after 3 h (dark gray)

(a)



(b)

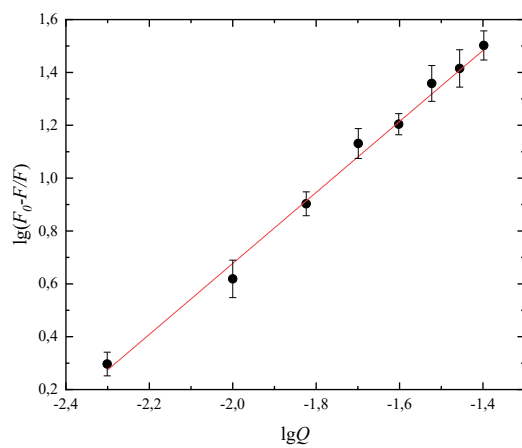


Fig. 11. HSA binding to ND-Dox (a) and ND-substance 1 (b) in Hill coordinates

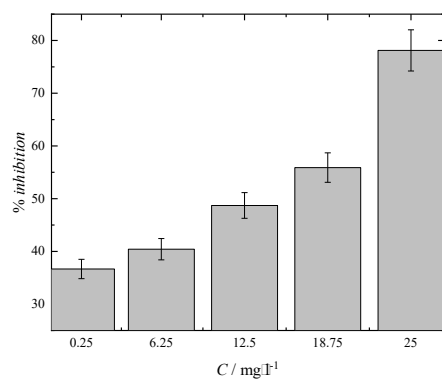


Fig 12. The dependence of the fraction of reduced radicals (% inhibition) on the concentration of ND-substance 1.

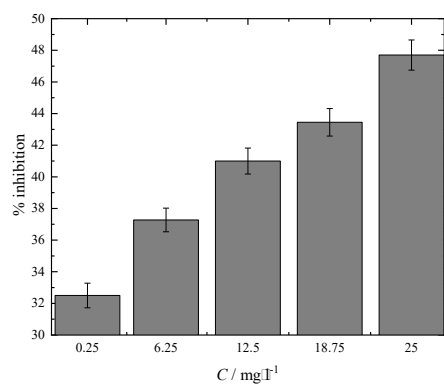
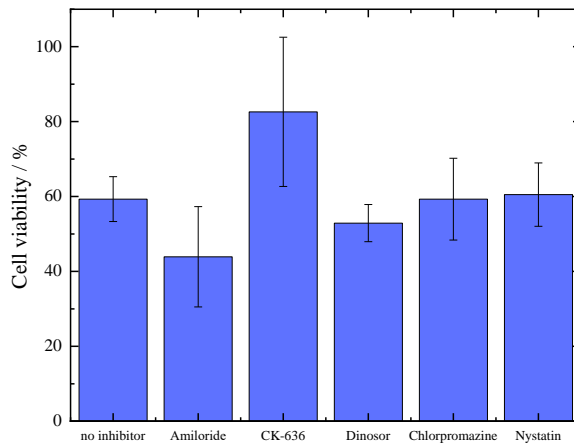


Fig 13. The dependence of the fraction of reduced radicals (% inhibition) on the concentration of ND-Dox.

(a)



(b)

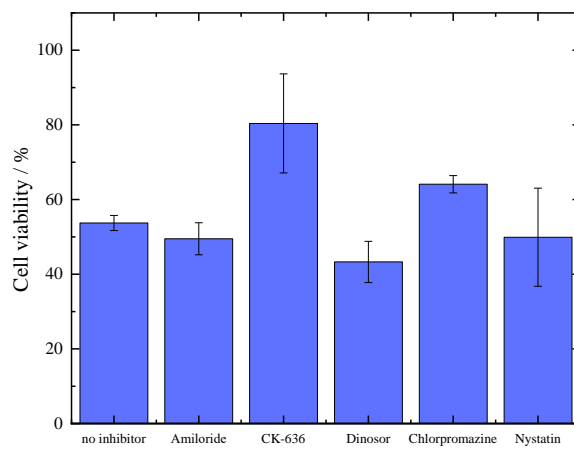
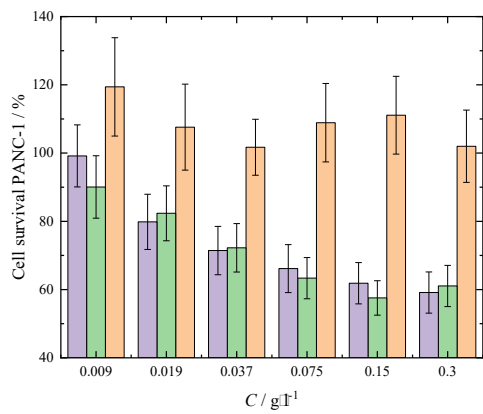
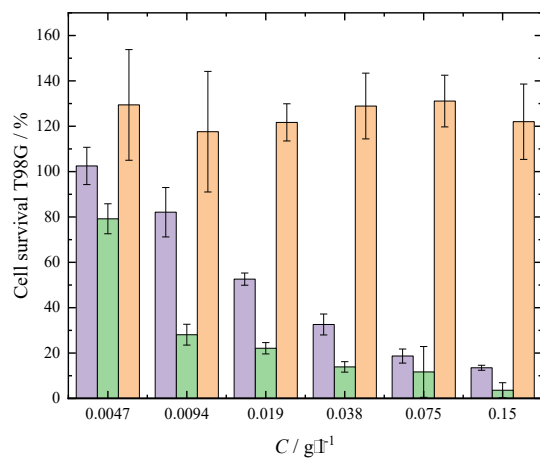


Fig 14. The Effect of endocytosis inhibitors on the survival of the HeLa cell line in the presence of conjugate (a) ND-substance 1 and (b) ND-Dox ( $C = 10\mu\text{M}$  in terms of individual cytostatic).

(a)



(b)



(c)

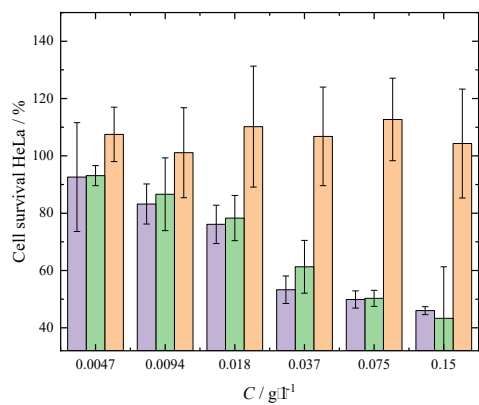
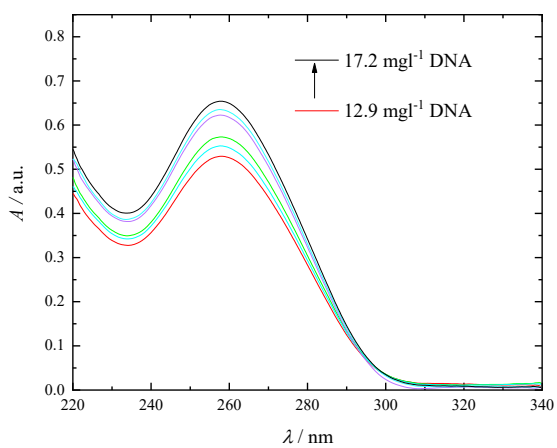


Fig 15. Cytotoxicity of ND (•), ND-substance 1 (•) and ND-Dox (•) towards PANC-1 (a), T98G (b), and HeLa (c) cell lines.



(a)



(b)

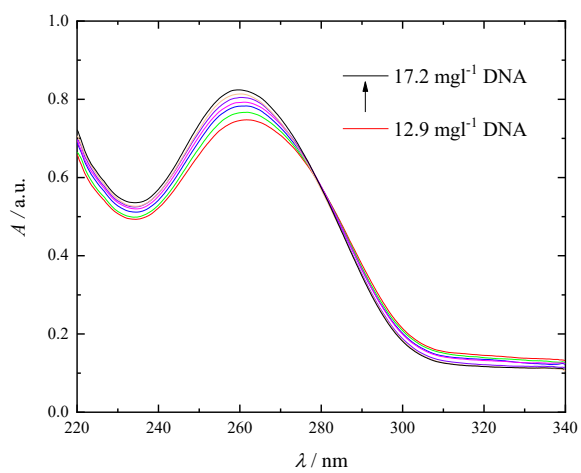
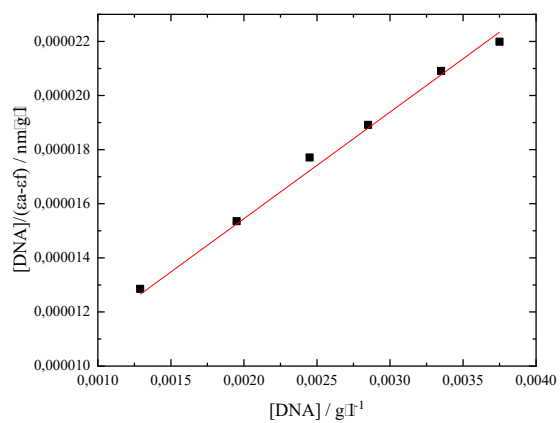


Fig 16. Absorption spectra of DNA with concentrations 12.9, 13.5, 14.1, 14.6, 15.0, 15.5, 15.9, 16.2, 16.6, 16.9,  $17.2 \text{ mg} \cdot \text{l}^{-1}$  in the presence ND-Dox (a), ND-substance 1 (b) with the concentrations  $5 \text{ mg} \cdot \text{l}^{-1}$ .

(a)



(b)

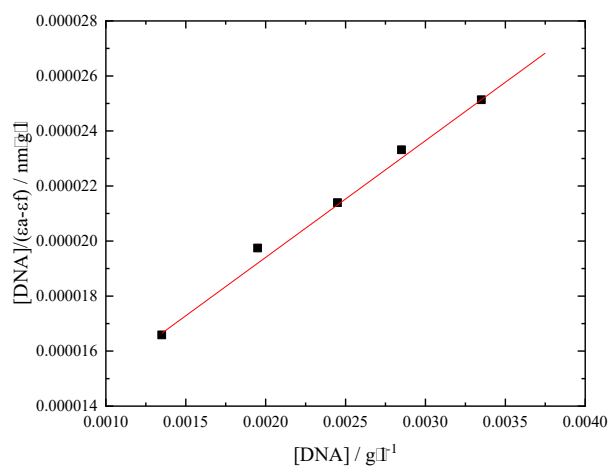


Fig 17. Dependence of  $[\text{DNA}]/(\epsilon_a - \epsilon_f)$  from  $[\text{DNA}]$  binding process of ND-Dox (a), ND-substance 1 (b) with DNA.

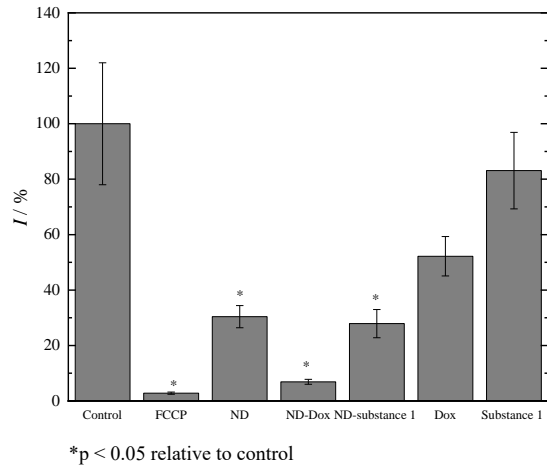


Fig. 18 The effect of ND, ND-Dox, ND-substance 1, Dox and Substance 1 on the mitochondrial membrane potential ( $\Delta\Psi_m$ ).

Formatted: Font: Not Bold